THE JOURNAL OF PHYSICAL CHEMISTRY C

Article

pubs.acs.org/JPCC

Elastic Modulus and Thermal Conductivity of Thiolene/TiO_2 Nanocomposites

Eugen Schechtel,[†] Yaping Yan,[‡] Xiangfan Xu,*[,‡] Yu Cang,[§] Wolfgang Tremel,[†] Zuyuan Wang,[§] Baowen Li,[∥] and George Fytas*[,§]

[†]Johannes Gutenberg University, Duesbergweg 10-14, 55128 Mainz, Germany

[‡]Center for Phononics and Thermal Energy Science, School of Physics and Engineering and Institute of Advanced Study, Tongji University, Shanghai 200092, China

[§]Max Planck Institute for Polymer Research, Ackermannweg 10, 55128 Mainz, Germany

[∥]Department of Mechanical Engineering, University of Colorado, Boulder 80309, United States

Supporting Information

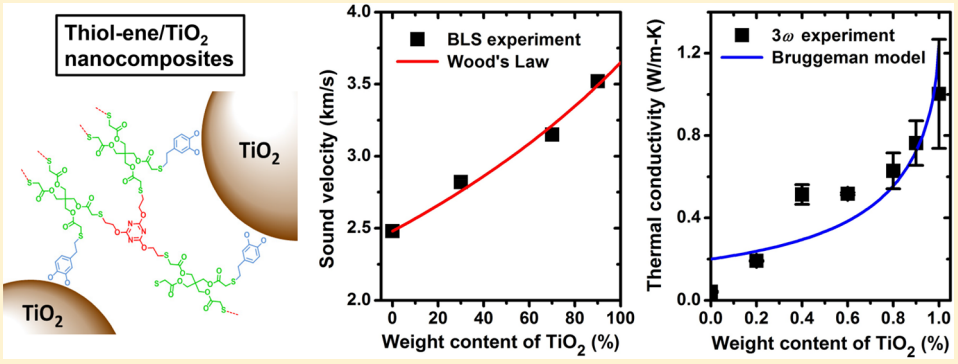

ABSTRACT: Metal oxide based polymer nanocomposites find diverse applications as functional materials, and in particular thiol-ene/TiO_2 nanocomposites are promising candidates for dental restorative materials. The important mechanical and thermal properties of the nanocomposites, however, are still not well understood. In this study, the elastic modulus and thermal conductivity of thiol-ene/TiO_2 nanocomposite thin films with varying weight fractions of TiO_2 nanoparticles are investigated by using Brillouin light scattering spectroscopy and 3ω measurements, respectively. As the TiO_2 weight fraction increases from 0 to 90%, the effective elastic longitudinal modulus of the films increases from 6.2 to 37.5 GPa, and the effective thermal conductivity from 0.04 to 0.76 W/m K. The former increase could be attributed to the covalent cross-linking of the nanocomposite constituents. The latter one could be ascribed to the addition of high thermal conductivity TiO_2 nanoparticles and the formation of possible conductive channels at high TiO_2 weight fractions. The linear dependence of the thermal conductivity on the sound velocity, reported for amorphous polymers, is not observed in the present nanocomposite system.

INTRODUCTION

Polymer nanocomposites are hybrid materials that integrate selected properties of both polymers and nanocolloids. It is currently a topic of intensive interest for both fundamental materials science and technology.[1,2] However, polymers and nanoparticles are hardly miscible in the absence of specific interactions due to depletion forces, leading to interesting nonequilibrium morphologies.[3] One strategy to obtain stable dispersions involves polymer grafts that results in matrix-free, one-component hybrid materials with novel mechanical, dielectric, thermal, or phononic properties.[4−6] A similar platform to fabricate homogeneous hybrid materials works by creating strong attachment of the nanoparticles to a network.[7]

The elastic modulus and thermal conductivity are two properties of paramount importance for material functions in a range of technologies. Polymers are low modulus (a few gigapascals)[6] and low thermal conductivity (0.1−0.3 W m^{-1} K^{-1})[8] materials compared with the inorganic counterparts. A promising strategy to increase these values is adding nanoparticles into the polymers—the design of polymer nanocomposites. While the elastic modulus depends mainly on the efficient packing and cohesive forces,[9−11] engineering of the thermal conductivity presents major challenges.[12,13] Besides the state of the dispersion, it is essential to have control over interfacial thermal resistance, which involves different characteristic length scales[14] and intermolecular interactions.[15] As for the latter issue, increasing the bonding strength of surfactants to the inorganic surface led to a strong increase of interfacial thermal

Received: August 23, 2017
Revised: October 4, 2017
Published: October 17, 2017

DOI: 10.1021/acs.jpcc.7b08425
J. Phys. Chem. C 2017, 121, 25568−25575

conductance.[16] A more recent work on thermal conduction in surfactant/semiconductor nanocrystals has further revealed the sensitivity of the effective thermal conductivity to the bonding strength of the molecular ligands.[17] The role of the polymeric tethers on the thermal conductivity has been recently addressed in the case of polymer/particle brush nanocomposites.[18] Favored enthalpic interactions between tethered and matrix polymer chains seem to be more relevant than the conceivable conformational nonuniformity of the tethered chains. However, there is limited literature on the mechanical and thermal properties of hybrid nanocomposites, and solid phenomenology necessary to develop theoretical concepts is also lacking.

In this work, we utilized a system that bridges the few molecular and polymer nanocomposites investigated so far. It is based on titanium dioxide (TiO_2, titania) nanoparticles, dispersed in a cross-linked organic matrix. Titania was chosen for the inorganic phase because of its use in a wide range of existing and emerging applications. It is not only an industrially important mass product (with numerous applications in health care)[19] but also the subject of current research on photovoltaics[20] and photocatalysis.[21,22] For most applications of nanoparticles in hybrid composites, it is beneficial to avoid particle agglomeration. To account for uniform dispersion and solid anchoring of the TiO_2 nanoparticles, the organic phase requires to be a cross-linked polymer matrix. These requirements can be readily met by thiol-ene (TE) click chemistry, which has proved to be a valuable platform in materials science, owing to its good adaptability and easy practicability.[23,24] Photoinitiated TE polymerizations neither require high curing temperatures, as epoxy resins do, nor suffer from oxygen inhibition or insufficient curing, which are common for photopolymerized acrylate-based resins.[25,26] Photopolymerized TE networks have already been used to fabricate hybrid nanocomposites by incorporating inorganic fillers like silicate clay minerals,[27] gold nanoparticles,[28,29] and TiO_2 particle powders.[30] However, none of these studies investigated nanocomposites with inorganic filler fractions exceeding 7 wt %. Due to the excellent dispensability of the nanoparticles used, the present approach allows fabrication of hybrid nanocomposites with inorganic filler fractions over the entire composition range (i.e., 0−100 wt % TiO_2 nanoparticles).

In this paper, we report on the effective elastic longitudinal moduli and thermal conductivities of TE/TiO_2 nanocomposite films at different nanoparticle weight fractions. The former are calculated as $M_{L,\,eff} = \rho_{eff} c^2_{L,\,eff}$, where ρ_{eff} is the effective density of the films and $c_{L,\,eff}$ is the effective longitudinal sound velocity obtained from Brillouin light scattering (BLS)[31−33] measurements; the latter are measured with the 3ω method.[15,34,35] To our knowledge, there are few reports on the relation between the sound velocity and thermal conductivity,[36,37] which are limited to bulk amorphous polymers and have demonstrated a linear dependence of the minimum thermal conductivity on the sound velocity. This work extends this investigation of the relation to polymer nanocomposite thin films. The results suggest that the covalent cross-linking of the nanocomposite constituents had a synergistic effect on sound propagation, yielding effective sound velocities of the nanocomposites that exceeded the value of the soft constituent (i.e., the TE network). The effective elastic longitudinal modulus increased monotonically from 6.2 to 37.5 GPa, as the wt % of TiO_2 nanoparticles increased from 0 to 90%. On the other hand, the corresponding effective thermal conductivity increased from 0.04 to 0.76 W/m K (by a factor of 18), due to the addition of high thermal conductivity TiO_2 nanoparticles and the formation of possible conductive channels at high TiO_2 weight fractions. These findings are potentially applicable for the development of improved dental resin composites, which require high inorganic filler loadings with strong anchoring of the nanoparticles to the polymer matrix to prevent loss of material to the human body. Indeed, both TiO_2 nanoparticles and TE resins have already been discussed as potential dental restorative materials in the literature.[38,39]

EXPERIMENTAL METHODS

Materials and Substrates. Unless otherwise stated, all chemicals were obtained from commercial suppliers and used without further purification. Pentaerythritol tetrakis (3-mercaptopropionate) (PETMP, >95%), 2,4,6-triallyloxy-1,3,5-triazine (TAOTA, 97%), and 2,2-dimethoxy-2-phenylacetophenone (DMPA, 99%) were obtained from Sigma-Aldrich. 4-Allylcatechol[40] and TiO_2 nanoparticles[41] were synthesized according to previously reported procedures with various modifications. The as-synthesized, oleic acid-stabilized nanoparticles are mostly of a spherical shape with a mean diameter of 6.5 ± 1.3 nm (see Figure S1a, b in the Supporting Information). The TiO_2 nanoparticles were refunctionalized with 4-allylcatechol in a biphasic reaction mixture. Details of the synthesis procedure can be found in the Supporting Information (Section D. Synthetic Procedure). Glass substrates of a size 13 × 13 mm^2 were cut from standard-sized microscope slides (75 × 26 mm^2), cleaned in Piranha solution (3:1 (v/v) conc. H_2SO_4/35 wt % H_2O_2) at 80 °C for 30 min, rinsed with Milli-Q water (18.2 MΩ cm), and dried in a stream of nitrogen. The same cleaning procedure was applied to the silicon substrates.

Film Preparation. Nanocomposite films were prepared by repeated spin coating of the premixed solutions. Prior to the spin coating, the allylcatechol-funtionalized TiO_2 nanoparticles were filtered through a series of syringe filters (3.1 μm glass fiber, 0.45 μm PET, and 0.2 μm PTFE) to remove dust particles and large aggregates from the solution. The filtered solution was stored in a dust-free amber glass vial with a screw cap. The exact concentration of the filtered solution was calculated from the remaining mass of an evaporated 100 μL aliquot (after several hours of drying at 80 °C). The concentration was found to be c = 84 mg/mL. A thiol-ene monomer stock solution was prepared by mixing pentaerythritol tetrakis (3-mercaptopropionate) (PETMP, 2.4433 g, 5.00 mmol, 1.00 equiv), 2,4,6-triallyloxy-1,3,5-triazine (TAOTA, 1.6626 g, 6.67 mmol, 1.33 equiv), and 2,2-dimethoxy-2-phenylacetophenone (DMPA, 0.0128 g, 0.05 mmol, 0.01 equiv) with toluene (40.0 mL). This mixture yielded a similar weight concentration with that of the nanoparticle solution ($c \approx$ 90 mg/mL). The stock solution was also filtered through a 0.2 μm PTFE syringe filter. Thiol−ene TiO_2 nanocomposites with varying TiO_2 contents were realized by mixing the nanoparticle and monomer stock solutions in different ratios. For example, for a sample with 70 wt % TiO_2 content, a volume ratio of 7:3 (TiO_2 solution:thiol-ene solution) was applied. The premixed solutions were then spin-cast to form nanocomposite films. In the spin coating, we used a dynamic dispense technique: first, the substrate was set to spin (acceleration: 5000 rpm/s) and allowed to reach a maximum speed of 5000 rpm; then, 30 μL premixed solution was quickly dispensed by using a 200 μL pipet into the center of the substrate (substrate size: 13 × 13

DOI: 10.1021/acs.jpcc.7b08425
J. Phys. Chem. C 2017, 121, 25568−25575

mm^2, spinning duration: 40 s). After spin coating, the samples were placed in a dust-free Petri dish and heated in an oven at 150 °C for 20 min to evaporate residual solvent. Subsequently, the Petri dish was placed under a UV lamp (366 nm, 8 W) for 5 min to ensure complete polymerization of the thiol-ene monomers. Each sequence of spin-coating and post-treatment resulted in a film layer with a thickness around 100 nm. The sequence was repeated multiple times to produce films of varying thicknesses to satisfy the requirements of the corresponding characterization techniques. For the Brillouin light scattering (BLS) characterization, which requires a film thickness of about 1 μm on a glass substrate, the nanocomposite films were fabricated by spin-coating a total of eight layers. For the 3ω technique, which works fine with thin films on silicon substrates, a pair of samples, consisting respectively of one and two layers, were fabricated for each composition.

Brillouin Light Spectroscopy. The sound velocities of the nanocomposite films are experimentally characterized by the Brillouin light scattering (BLS) spectroscopy. BLS is a nondestructive and powerful tool to probe the hypersonic phonon propagation, which utilizes the scattering of an incident probing laser beam by phonons in a specific direction. The phonon wave vector, $\mathbf{q}$, is determined by the scattering geometry as $\mathbf{q} = \mathbf{k}_s - \mathbf{k}_i$, where $\mathbf{k}_s$ and $\mathbf{k}_i$ are the wave vectors of the scattered and incident light, respectively. All BLS measurements in this study are conducted in the transmission geometry. In this geometry, the probing phonons propagate in the film plane, and the wavenumber, being independent of the refractive index, can be expressed as $q = \frac{4\pi}{\lambda}\sin\frac{\theta}{2}$, where λ is the wavelength of the incident beam (i.e., 532 nm) and θ is the scattering angle. The inelastic interactions of the incident light with the activated phonons are represented by the frequency shift, $f(q)$, of the BLS spectra, which are resolved by a six-pass tandem Fabry–Pérot interferometer at the hypersonic frequency range. The longitudinal (VV) and transverse (VH) displacements are selected by the polarizations, where VV and VH represent vertically and horizontally polarized lasers with respect to the scattering plane, respectively.

3ω Method. A thin Cr/Au (5 nm/50 nm) electrode, 50 μm wide and 1 mm long, was deposited onto each TE/TiO_2 film using a metal mask and thermal evaporation. To carry out the 3ω measurement, an ac current with a frequency of 1ω was applied to the Cr/Au electrode, which introduces a fluctuation of the temperature and consequently the electrical resistance of the electrode with a frequency of 2ω, when the temperature increase is sufficiently small. The temperature increase of the electrode can be calculated as $T_{2\omega} = 2\frac{dT}{dR}\frac{R}{V_{1\omega}}V_{3\omega}$, where R is the average electrical resistance of the Cr/Au electrode, dR/dT is the temperature coefficient of the resistance, and $V_{1\omega}$ and $V_{3\omega}$ are the measured 1ω and 3ω voltages on the electrodes, respectively. To measure the out-of-plane thermal conductivity of the TE/TiO_2 film, a differential 3ω measurement was carried out. Two films with different thicknesses were used (see the inset of Figure 4a). When the half-width of electrode is much larger than the thickness of the TE/TiO_2 film but much smaller than the heat penetration depth, the heat transfer from the electrode, across the sample film, and into the Si substrate can be reasonably approximated as one-dimensional (1D). As a result, the thermal conductivity, k, of the TE/TiO_2 film can be calculated as $k = \frac{P\cdot h}{\Delta T_{2\omega}\cdot A_c}$, where P is the heating power, h is the thickness deference between thin and thick films, A_c is the cross-sectional area of the heat path, and $\Delta T_{2\omega}$ is the temperature difference between the thin and thick films.

RESULTS AND DISCUSSION

Nanocomposite Films. The nanocomposite films were prepared on glass or silicon substrates by repeated spin-coating of premixed solutions of TiO_2 nanoparticles and TE monomers in the desired ratios. To chemically link the TiO_2 nanoparticles to the TE polymer matrix, short bifunctional catecholic anchors (derived from eugenol, a natural odorant found in clove oil[40]) were first attached to the TiO_2 nanoparticles, as illustrated in Figure 1a. This treatment is similar to the versatile catechol chemistry, which enables marine organisms (e.g., mussels) to virtually adhere to any surface.[42−44] The terminal double bonds at the other ends of the anchor molecules serve as connection points to the cross-linked TE network (see Figure 1b).[45] After spin-coating and drying, the nanocomposite films were exposed to UV radiation (366 nm, 8 W) for 5 min. As the thermal diffusion time of each spin-coating layer can be estimated to be on the order of 10−100 ns, the duration of UV exposure should be sufficient to ensure complete polymerization of the TE monomers.

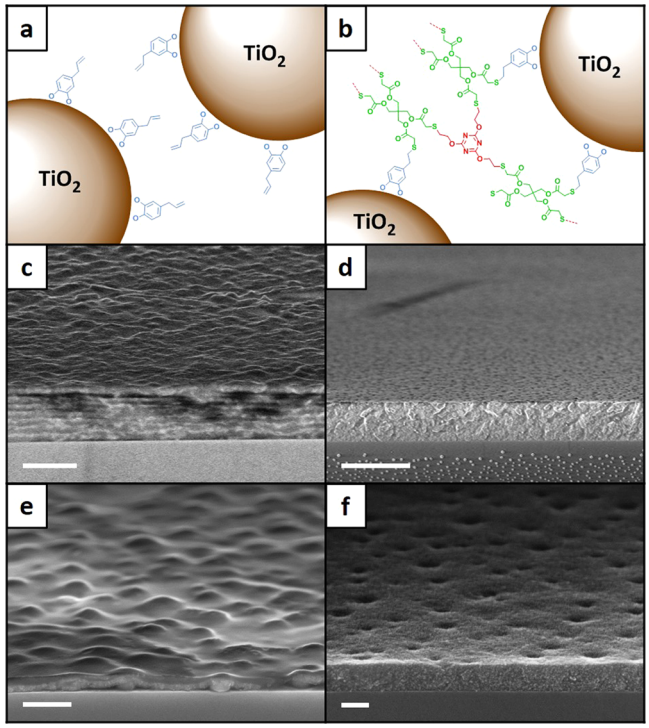

Figure 1. (a) Schematic of a pure TiO_2 nanoparticle film, where the surface-refunctionalized TiO_2 nanoparticles are not cross-linked. (b) Schematic of a TE/TiO_2 nanocomposite film, where the surface-refunctionalized TiO_2 nanoparticles are covalently attached to the TE polymer network. (c) An eight-layer TE/TiO_2 nanocomposite film containing 30 wt % TiO_2. (d) An eight-layer TE/TiO_2 nanocomposite film containing 90 wt % TiO_2. (e) A two-layer TE/TiO_2 nanocomposite film containing 40 wt % TiO_2. (f) A two-layer TiO_2 nanoparticle film containing 100 wt % TiO_2. (c) and (d) are supported on glass substrates and used in the BLS measurements. (e) and (f) are supported on Si substrates and used in the 3ω measurements. The scale bars are (c) 1 μm, (d) 2 μm, (e) 500 nm, and (f) 100 nm.

DOI: 10.1021/acs.jpcc.7b08425
J. Phys. Chem. C 2017, 121, 25568−25575

The nanocomposite films were characterized by using scanning electron microscopy (SEM). Figure 1c, d shows two thick films supported on glass substrates and used in the BLS measurements. They contain 30 and 90 wt % of TiO_2 nanoparticles respectively, and both of them have a thickness around 1 μm. Figure 1e, f shows two thin films supported on Si substrates and used in the 3ω measurements. They contain 80 and 100 wt % of TiO_2 nanoparticles, respectively. At a low wt % of TiO_2 nanoparticles, the interfaces between consecutive spin-coating layers are discernible (see Figure 1c, e). At a large wt % of TiO_2 nanoparticles, the interfaces become indistinguishable (see Figure 1d, f), leading to a homogeneous film. All nanocomposite films show some degree of surface roughness, especially for the thin films with a low wt % of TiO_2 nanoparticles. Additional SEM images can be found in the Supporting Information (Section C. SEM Images of Nanocomposite Films). Besides being used to check the uniformity and homogeneity of the nanocomposite films, the SEM images were also used to determine the film thicknesses.

We point out that some of the thin nanocomposite films have a relatively high level of roughness (see Figures 1e, S3b, S4c), which could be caused by the evaporation of the solvent in the drying process. Further studies are needed to understand the mechanisms and to optimize the fabrication parameters (e.g., UV light intensity, oven temperature) to achieve a lower level of roughness. Nevertheless, in the thermal conductivity measurements, the roughness effect should be insignificant, as we always used two films with different thicknesses (see Figure 4a); for the BLS experiments, thick films were employed.

Elastic Longitudinal Modulus. All films used in the BLS experiments consisted of eight consecutive layers to achieve thicknesses about 1 μm, except for the thick bulk TE films used for depolarized BLS measurements. This thickness is required to ensure a linear acoustic behavior[46] for in-plane phonon propagation by fulfilling the condition, $qh \gg 1$, where q is wavenumber and h is the film thickness. As the elastic properties of the bulk TE and TiO_2 are necessary information for understanding the mechanical behaviors of the nanocomposites, the bulk TE and TiO_2 nanoparticle films were first examined. The BLS spectra of these films were recorded at a given q = 0.013 55 nm^{-1} in the polarized (for both the bulk TE and TiO_2 films) and depolarized light polarizations (for the bulk TE film only), as shown in Figure 2a. The single Lorentzian representation of the BLS spectra indicated a homogeneous medium in both the bulk TE and TiO_2 films prepared by the spin-coating method, as also confirmed by the SEM images in Figure 1f for the latter. Note that for spatially inhomogeneous polymer nanocomposites two acoustic phonons at a given q can be observed.[47] Due to the cross-linked TE network, the bulk TE film displays measurable depolarized BLS spectra, allowing for the measurement of the transverse sound velocity, c_T. This transverse mode in the depolarized spectra is only measured in the thick bulk TE films, as the mode is too weak to be detected in the other thin nanocomposite films. The frequency, f, obtained from the Lorentzian peaks increases linearly with the wavenumber, q, as seen in Figure 2b and expected for acoustic phonon propagation.

The sound velocities, $c = \frac{d\omega}{dq} = \frac{2\pi df}{dq}$, obtained from the slope of the linear relations, $f(q) \sim q$, are $c_{L,\,TE}$ = 2480 ± 12 m/s and $c_{T,\,TE}$ = 1000 ± 15 m/s for the pure TE thin film, and $c_{L,\,TiO2}$ = 3070 ± 30 m/s for the pure TiO_2 thin film; the subscripts, L and T, stand for longitudinal and transverse,

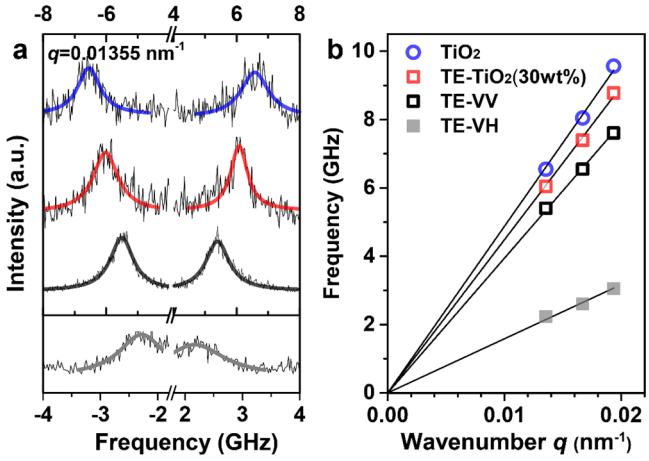

Figure 2. (a) Brillouin light scattering (BLS) spectra for in-plane phonon propagation at q = 0.013 55 nm^{-1}. The polarized spectra (in the range of −8 to 8 GHz) are represented by single Lorentzian peaks for the bulk TE (black line) and TE/TiO_2 nanocomposite (red line for TiO_2-30 wt % and blue line for TiO_2 nanoparticle films). The depolarized BLS spectrum of the bulk TE (in the range of −4 to 4 GHz) is also represented by a single Lorentzian peak (gray line), indicating a weak cross-linked structure of TE matrix. (b) The phonon dispersion relations for these three compositions shown with the same color are linear, $f(q) \sim q$, as indicated by the four black lines.

respectively. Based on the $c_{L,\,TE}$ and $c_{T,\,TE}$, the Poisson's ratio, $\nu = \frac{x-2}{2(x-1)}$ with $x = \left(\frac{c_{L,TE}}{c_{T,TE}}\right)^2$, turns out to be about 0.4, and thus suggests a weakly cross-linked and soften matrix. The relatively low $c_{L,\,TiO2}$ compared with the value for bulk crystalline anatase TiO_2 film (with a longitudinal sound velocity of around 8880 m/s[48]) could be attributed to the granular structure of the TiO_2 nanoparticle film. Similar to the BLS spectra of the bulk TE and TiO_2 nanoparticle films, the BLS spectra of the nanocomposite film with 30 wt % of TiO_2 nanoparticles show a single longitudinal mode (see Figure 2a), suggesting a homogeneous medium.[47] The corresponding longitudinal effective medium sound velocity $c_{L,\,eff}$, estimated from the linear dispersion relation (see Figure 2b) of the film, is 2820 ± 20 m/s, which falls between the sound velocities of the pure TE and TiO_2 nanoparticle films.

To gain more insights, the sound velocities were represented by Wood's law[49,50] as

$$\frac{1}{M_{L,\mathrm{eff}}} = \frac{\phi_{TiO_2}}{M_{L,TiO_2}} + \frac{1-\phi_{TiO_2}}{M_{L,TE}} \quad (1)$$

which can be combined with $M_L = \rho c_L^2$, $\rho_{eff} = \rho_{TiO_2}\phi_{TiO_2} + \rho_{TE}(1 - \phi_{TiO_2})$, and $\phi_{TiO2} = (\rho_{TE}w_{TiO2})/(\rho_{TE}w_{TiO2} + \rho_{TiO2}(1 - w_{TiO2}))$ to give

$$c_{L,\mathrm{eff}} = \frac{c_{L,TiO_2}c_{L,TE}[\rho_{TE}w_{TiO_2} + \rho_{TiO_2}(1-w_{TiO_2})]}{[\rho_{TE}^2c_{L,TE}^2w_{TiO_2} + \rho_{TiO_2}^2c_{L,TiO_2}^2(1-w_{TiO_2})]^{0.5}} \quad (2)$$

Here, M is the longitudinal modulus, and ϕ_{TiO_2} and w_{TiO_2} are the volume and weight fractions of the TiO_2 nanoparticles, respectively. In the least-squares fitting with eq 2, which expresses $c_{L,\,eff}$ as a function of ϕ_{TiO_2}, the following materials properties were fixed: ρ_{TE} = 1000 kg/m^3 and $c_{L,\,TE}$ = 2480 m/s, whereas ρ_{TiO_2} and $c_{L,\,TiO_2}$ were treated as fitting parameters. The

DOI: 10.1021/acs.jpcc.7b08425
J. Phys. Chem. C 2017, 121, 25568−25575

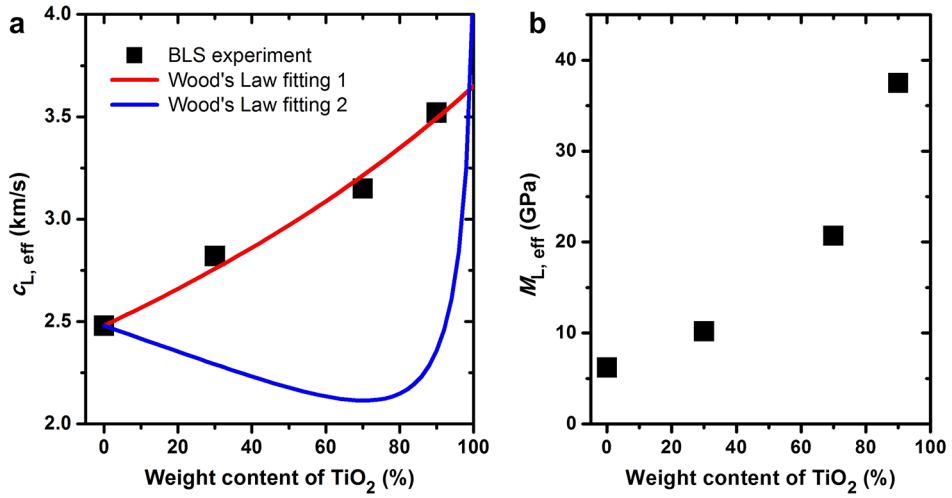

Figure 3. (a) Effective longitudinal sound velocity of the TE/TiO_2 nanocomposites at varying weight fraction of the TiO_2 nanoparticles. The Wood's law fitting based on eq 2 was conducted with two sets of adjustable values of the density and sound velocity of TiO_2 (red line: ρ_{TiO_2} = 870 kg/m^3 and $c_{L,\,TiO_2}$ = 3650 m/s; blue line: ρ_{TiO_2} = 3900 kg/m^3 and $c_{L,\,TiO_2}$ = 8880 m/s). (b) Computed effective elastic longitudinal modulus of the TE/TiO_2 nanocomposites as a function of the weight fraction of the TiO_2 nanoparticles (see text).

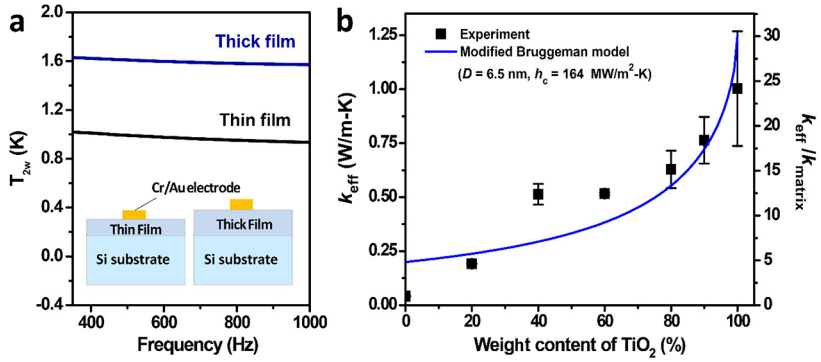

Figure 4. Effective thermal conductivity of TE/TiO_2 nanocomposites at varying wt % of TiO_2 nanoparticles. The experimental data from the 3ω measurements (solid circles) are represented (blue solid line) by a modified Bruggeman model (eq 3).

experimental $c_{L,\,eff}$ data are shown in Figure 3a, which also includes the best fit with ρ_{TiO_2} = 870 kg/m^3 and $c_{L,\,TiO_2}$ = 3650 m/s, and another fit with the bulk TiO_2 film values, ρ_{TiO_2} = 3900 kg/m^3 and $c_{L,\,TiO_2}$ = 8880 m/s. It is surprising that such a low ρ_{TiO_2} (even lower than ρ_{TE}) is needed to capture the experimental composition dependence of the effective medium sound velocity with Wood's law. To check whether the TiO_2 nanoparticles are porous, XRD measurements were conducted to analyze their crystallinity. The X-ray diffraction pattern shown in Figure S2, however, confirms that the TiO_2 nanoparticles are indeed crystalline, without pores inside. We note that in a previous report on the sound velocity of PMMA/$BaTiO_3$ nanocomposites,[9] a $c_{L,\,eff}$ trend in better agreement with the Wood's law's prediction is observed. If ρ_{TiO_2} is fixed at 3900 kg/m^3 and $c_{L,\,TiO_2}$ at 8880 m/s, the trend of the fitted curve deviates from the experimental data but shows a similar trend with the results for the PMMA/$BaTiO_3$ nanocomposites.[9] The surprisingly low ρ_{TiO_2}, required to represent the experimental $c_{L,\,eff}$, could be attributed to the specific interfacial effects (i.e., covalent cross-linking) in this polymer nanocomposite. In Figure 3b, we show the variation of the effective elastic longitudinal modulus with the TiO_2 wt %. It is seen that $M_{L,\,eff}$ increases monotonically from 6.2 to 37.5 GPa, as the TiO_2 wt % increases from 0 to 90%. Note that ρ_{TiO_2} = 3900 kg/m^3 was used to calculate ρ_{eff} in the calculations of $M_{L,\,eff}$.

Thermal Conductivity. The cross-plane thermal conductivities of the TE/TiO_2 nanocomposite films were measured with the differential 3ω method.[34] To eliminate the effects of the interfacial thermal resistances (i.e., between the Cr/Au electrode and TE/TiO_2 film, and between the TE/TiO_2 film and silicon wafer) and the thermal resistance of the silicon substrate, two TE/TiO_2 samples with different thicknesses (e.g., h_1 and h_2; $h_1 < h_2$) were fabricated (see Figure 4a). The temperature vs. ac current frequency responses of the two samples can be used to calculate the thermal conductivity corresponding to a film of thickness, $(h_2 - h_1)$ (refer to the Methods section for more details). The experimental thermal conductivities are shown in Figure 4b, as a function of the TiO_2 weight fraction. For the pure TE film, the measured thermal conductivity (0.04 W/m K) is lower than the typical values (0.1–0.3 W/m K[8]) of amorphous polymers. With increasing fraction of the TiO_2 nanoparticles, the thermal conductivity of the nanocomposite increases monotonically and for the 100 wt % TiO_2 nanoparticle film reaches 1.0 ± 0.3 W/m K, comparable to that of amorphous TiO_2 thin film and TiO_2 nanoparticles.[51,52]

DOI: 10.1021/acs.jpcc.7b08425
J. Phys. Chem. C 2017, 121, 25568–25575

The thermal conductivities were fitted with a modified Bruggeman model[53,54] as

$$(1-\phi_{TiO_2})^3 = \left(\frac{k_{TE}}{k_{eff}}\right)^{(1+2\alpha)/(1-\alpha)} \left(\frac{k_{eff}-k_{TiO_2}(1-\alpha)}{k_{TE}-k_{TiO_2}(1-\alpha)}\right)^{3/(1-\alpha)} \quad (3)$$

where $\alpha = 2k_{TE}/(Dh_c)$ is a parameter depending on the thermal conductivity of the TE matrix (k_{TE}), the diameter of the TiO_2 nanoparticles (D), and the interfacial thermal conductance (h_c) between the TiO_2 nanoparticles and the TE matrix. This model by definition takes into account the interactions between the nanoparticles and the matrix, as well as the effect of the interfacial thermal resistance. In the fitting, the following parameters were adopted:[52] D = 6.5 nm, k_{TE} = 0.2 W/m K, and k_{TiO_2} = 2.0 W/m K. Note that the thermal conductivity of the TE matrix is set as that of a typical polymer, instead of the experimentally measured value for the pure TE film. Based on the representation of the experimental data shown in Figure 4b, the thermal conductivity trend is well captured, confirming the good predictability of the model for the thermal conductivity of composites with high particle filling fractions.[53,54] From the best fit, the interfacial thermal conductance was determined to be 164 MW/m^{2}K, which falls in the range of 10^7–10^8 W/m^2 K for typical interfacial thermal conductances between organic/inorganic interfaces.[14,55] Since the TiO_2 nanoparticles are covalently linked to the TE polymer matrix, this relatively high interfacial thermal conductance is expected.

By comparing the relative increases of the sound velocities in Figure 3a and the thermal conductivities in Figure 4b, it is seen that as the wt % of the TiO_2 nanoparticles increases from 0 to 90%, the $c_{L,\,eff}$ increases by around 40%, but the k_{eff} increases by a factor of 18. From the kinetic theory of thermal conductivity, it is known that $k_{eff} = \frac{1}{3}C_{eff}v_{g,eff}\Lambda_{eff}$, where C_{eff}, $v_{g,\,eff}$, and Λ_{eff} are the effective specific heat, phonon group velocity, and phonon mean free path, respectively. Since the specific heat of polymers is typically around 1000 J/kg K[56] and the heat capacity of TiO_2 nanoparticles with a diameter of 6.5 nm is 850 J/kg K[57] (obtained from extrapolation), the change in the effective specific heat caused by increasing the wt % of TiO_2 nanoparticles is expected to be insignificant. For the effective phonon group velocity, it can be reasonably assumed to be equal to the sound velocity and thus increases by 42% as the wt % of the TiO_2 nanoparticles increases from 0 to 90%. Therefore, the increase of the thermal conductivity with the increasing TiO_2 wt % is primarily due to the increase in the effective mean free path. In fact, it has been shown that at high filling fractions, conductive channels could be formed by the nanoparticles to allow for effective thermal transport (the so-called percolation phenomenon).[54,58]

CONCLUSIONS

This study investigates the elastic modulus and thermal conductivity of thiol-ene/TiO_2 nanocomposite thin films with varying weight fractions of TiO_2 nanoparticles by using the Brillouin light spectroscopy and 3ω measurements, respectively. The effective elastic longitudinal moduli of the films are found to increase with the weight fraction of the TiO_2 nanoparticles, from 6.2 GPa at 0 wt % of TiO_2 to 37.5 GPa at 90 wt % of TiO_2. The corresponding effective thermal conductivity shows a much more significant increase, from 0.04 to 0.76 W/m K (by a factor of 18). The increase of the modulus is not predicted by the effective medium model, probably due to the specific interactions between the components of the nanocomposites. The strong composition dependence of the effective thermal conductivity can be captured by the effective medium model by using a physically meaningful interfacial thermal conductance. However, the relation between the thermal conductivity and sound velocity is found to be nonlinear, in contrast to the linear relation observed in amorphous polymers. The pronounced enhancement of the effective thermal conductivity could be ascribed to the addition of high thermal conductivity TiO_2 nanoparticles and the formation of possible conductive channels at high TiO_2 weight fractions.

ASSOCIATED CONTENT

Supporting Information

The Supporting Information is available free of charge on the ACS Publications website at DOI: 10.1021/acs.jpcc.7b08425.

Size and shape of TiO_2 nanoparticles, crystallinity of TiO_2 nanoparticles, SEM images of nanocomposite films, and synthetic procedure (PDF)

AUTHOR INFORMATION

Corresponding Authors

*E-mail: xuxiangfan@tongji.edu.cn.
*E-mail: fytas@mpip-mainz.mpg.de.

ORCID

Xiangfan Xu: 0000-0001-7163-4957
Wolfgang Tremel: 0000-0002-4536-994X

Author Contributions

The manuscript was written through contributions of all authors. All authors have given approval to the final version of the manuscript.

Notes

The authors declare no competing financial interest.

ACKNOWLEDGMENTS

E.S. is grateful to the Max Planck Graduate Center (MPGC) for financial support. G.F. acknowledges the hospitality of the Center for Phononics and Thermal Energy Science at Tongji University. Z.W. acknowledges Dr. Bahram Djafari-Rouhani for fruitful discussions, and X.X. was supported by National Key R&D Program of China (No. 2017YFB0406000). This work was supported by ERC (SmartPhon No. 694977).

REFERENCES

(1) Kumar, S. K.; Krishnamoorti, R. Nanocomposites: Structure, Phase Behavior, and Properties. *Annu. Rev. Chem. Biomol. Eng.* **2010**, *1*, 37–58.

(2) Varol, H. S.; Meng, F.; Hosseinkhani, B.; Malm, C.; Bonn, D.; Bonn, M.; Zaccone, A.; Parekh, S. H. Nanoparticle Amount, and Not Size, Determines Chain Alignment and Nonlinear Hardening in Polymer Nanocomposites. *Proc. Natl. Acad. Sci. U. S. A.* **2017**, *114*, E3170–E3177.

(3) Akcora, P.; Liu, H.; Kumar, S. K.; Moll, J.; Li, Y.; Benicewicz, B. C.; Schadler, L. S.; Acehan, D.; Panagiotopoulos, A. Z.; Pryamitsyn, V.; et al. Anisotropic Self-Assembly of Spherical Polymer-Grafted Nanoparticles. *Nat. Mater.* **2009**, *8*, 354–359.

DOI: 10.1021/acs.jpcc.7b08425
J. Phys. Chem. C 2017, 121, 25568–25575

(4) Grabowski, C. A.; Koerner, H.; Meth, J. S.; Dang, A.; Hui, C. M.; Matyjaszewski, K.; Bockstaller, M. R.; Durstock, M. F.; Vaia, R. A. Performance of Dielectric Nanocomposites: Matrix-Free, Hairy Nanoparticle Assemblies and Amorphous Polymer−Nanoparticle Blends. *ACS Appl. Mater. Interfaces* **2014**, *6*, 21500−21509.
(5) Kim, S. A.; Mangal, R.; Archer, L. A. Relaxation Dynamics of Nanoparticle-Tethered Polymer Chains. *Macromolecules* **2015**, *48*, 6280−6293.
(6) Alonso-Redondo, E.; Schmitt, M.; Urbach, Z.; Hui, C. M.; Sainidou, R.; Rembert, P.; Matyjaszewski, K.; Bockstaller, M. R.; Fytas, G. A New Class of Tunable Hypersonic Phononic Crystals Based on Polymer-Tethered Colloids. *Nat. Commun.* **2015**, *6*, 8309.
(7) Fuhrer, R.; Athanassiou, E. K.; Luechinger, N. A.; Stark, W. J. Crosslinking Metal Nanoparticles into the Polymer Backbone of Hydrogels Enables Preparation of Soft, Magnetic Field-Driven Actuators with Muscle-like Flexibility. *Small* **2009**, *5*, 383−388.
(8) Yang, Y. Thermal Conductivity. In *Physical Properties of Polymers Handbook*; Mark, J. E., Ed.; Springer: New York, 2007; pp 155−163.
(9) Alonso-Redondo, E.; Gueddida, A.; Huesmann, H.; El Abouti, O.; Tremel, W.; El Boudouti, E. H.; Djafari-Rouhani, B.; Fytas, G. Direction-Dependent Elastic Properties and Phononic Behavior of PMMA/$BaTiO_3$ Nanocomposite Thin Films. *J. Chem. Phys.* **2017**, *146*, 203325.
(10) Mirigian, S.; Schweizer, K. S. Elastically Cooperative Activated Barrier Hopping Theory of Relaxation in Viscous Fluids. II. Thermal Liquids. *J. Chem. Phys.* **2014**, *140*, 194507.
(11) Mbanga, B. L.; Iyer, B. V. S.; Yashin, V. V.; Balazs, A. C. Tuning the Mechanical Properties of Polymer-Grafted Nanoparticle Networks through the Use of Biomimetic Catch Bonds. *Macromolecules* **2016**, *49*, 1353−1361.
(12) Neogi, S.; Reparaz, J. S.; Pereira, L. F. C.; Graczykowski, B.; Wagner, M. R.; Sledzinska, M.; Shchepetov, A.; Prunnila, M.; Ahopelto, J.; Sotomayor-Torres, C. M.; et al. Tuning Thermal Transport in Ultrathin Silicon Membranes by Surface Nanoscale Engineering. *ACS Nano* **2015**, *9*, 3820−3828.
(13) Volz, S.; Ordonez-Miranda, J.; Shchepetov, A.; Prunnila, M.; Ahopelto, J.; Pezeril, T.; Vaudel, G.; Gusev, V.; Ruello, P.; Weig, E. M.; et al. Nanophononics: State of the art and perspectives. *Eur. Phys. J. B* **2016**, *89*, 15.
(14) Putnam, S. A.; Cahill, D. G.; Ash, B. J.; Schadler, L. S. High-Precision Thermal Conductivity Measurements as a Probe of Polymer/Nanoparticle Interfaces. *J. Appl. Phys.* **2003**, *94*, 6785−6788.
(15) Kim, G.-H.; Lee, D.; Shanker, A.; Shao, L.; Kwon, M. S.; Gidley, D.; Kim, J.; Pipe, K. P. High Thermal Conductivity in Amorphous Polymer Blends by Engineered Interchain Interactions. *Nat. Mater.* **2015**, *14*, 295−300.
(16) Losego, M. D.; Grady, M. E.; Sottos, N. R.; Cahill, D. G.; Braun, P. V. Effects of Chemical Bonding on Heat Transport across Interfaces. *Nat. Mater.* **2012**, *11*, 502−506.
(17) Ong, W.-L.; Rupich, S. M.; Talapin, D. V.; McGaughey, A. J. H.; Malen, J. A. Surface Chemistry Mediates Thermal Transport in Three-Dimensional Nanocrystal Arrays. *Nat. Mater.* **2013**, *12*, 410−415.
(18) Mahoney, C.; Hui, C. M.; Majumdar, S.; Wang, Z.; Malen, J. A.; Tchoul, M. N.; Matyjaszewski, K.; Bockstaller, M. R. Enhancing Thermal Transport in Nanocomposites by Polymer-Graft Modification of Particle Fillers. *Polymer* **2016**, *93*, 72−77.
(19) Chen, X.; Mao, S. S. Titanium Dioxide Nanomaterials: Synthesis, Properties, Modifications, and Applications. *Chem. Rev.* **2007**, *107*, 2891−2959.
(20) Shakeel Ahmad, M.; Pandey, A. K.; Abd Rahim, N. Advancements in the Development of TiO_2 Photoanodes and Its Fabrication Methods for Dye Sensitized Solar Cell (DSSC) Applications. A Review. *Renewable Sustainable Energy Rev.* **2017**, *77*, 89−108.
(21) Schneider, J.; Matsuoka, M.; Takeuchi, M.; Zhang, J.; Horiuchi, Y.; Anpo, M.; Bahnemann, D. W. Understanding TiO_2 Photocatalysis: Mechanisms and Materials. *Chem. Rev.* **2014**, *114*, 9919−9986.
(22) Zhang, Y.; Jiang, Z.; Huang, J.; Lim, L. Y.; Li, W.; Deng, J.; Gong, D.; Tang, Y.; Lai, Y.; Chen, Z. Titanate and Titania Nanostructured Materials for Environmental and Energy Applications: A Review. *RSC Adv.* **2015**, *5*, 79479−79510.
(23) Hoyle, C. E.; Lowe, A. B.; Bowman, C. N. Thiol-Click Chemistry: A Multifaceted Toolbox for Small Molecule and Polymer Synthesis. *Chem. Soc. Rev.* **2010**, *39*, 1355−1387.
(24) Hoyle, C. E.; Bowman, C. N. Thiol-Ene Click Chemistry. *Angew. Chem., Int. Ed.* **2010**, *49*, 1540−1573.
(25) Hoyle, C. E.; Lee, T. Y.; Roper, T. Thiol-Enes: Chemistry of the Past with Promise for the Future. *J. Polym. Sci., Part A: Polym. Chem.* **2004**, *42*, 5301−5338.
(26) Li, Q.; Zhou, H.; Hoyle, C. E. The Effect of Thiol and Ene Structures on Thiol−ene Networks: Photopolymerization, Physical, Mechanical and Optical Properties. *Polymer* **2009**, *50*, 2237−2245.
(27) Colucci, G.; Mana, S.; Conzatti, L.; Sangermano, M. Hybrid Organic−Inorganic Silicate/Thiol−Ene Photocured Coatings. *Surf. Coat. Technol.* **2012**, *206*, 2719−2724.
(28) Phillips, J. P.; Mackey, N. M.; Confait, B. S.; Heaps, D. T.; Deng, X.; Todd, M. L.; Stevenson, S.; Zhou, H.; Hoyle, C. E. Dispersion of Gold Nanoparticles in UV-Cured, Thiol−Ene Films by Precomplexation of Gold−Thiol. *Chem. Mater.* **2008**, *20*, 5240−5245.
(29) Boyd, D. A.; Naciri, J.; Fontana, J.; Pacardo, D. B.; Shields, A. R.; Verbarg, J.; Spillmann, C. M.; Ligler, F. S. Facile Fabrication of Color Tunable Film and Fiber Nanocomposites via Thiol Click Chemistry. *Macromolecules* **2014**, *47*, 695−704.
(30) Jefferson, L. U.; Netchaev, A. D.; Jefcoat, J. A.; Windham, A. D.; McFarland, F. M.; Guo, S.; Buchanan, R. K.; Buchanan, J. P. Preparation and Characterization of Polyhedral Oligomeric Silsesquioxane-Containing, Titania-Thiol-Ene Composite Photocatalytic Coatings, Emphasizing the Hydrophobic−Hydrophilic Transition. *ACS Appl. Mater. Interfaces* **2015**, *7*, 12639−12648.
(31) Gomopoulos, N.; Maschke, D.; Koh, C. Y.; Thomas, E. L.; Tremel, W.; Butt, H.-J.; Fytas, G. One-Dimensional Hypersonic Phononic Crystals. *Nano Lett.* **2010**, *10*, 980−984.
(32) Schneider, D.; Liaqat, F.; El Boudouti, E. H.; El Hassouani, Y.; Djafari-Rouhani, B.; Tremel, W.; Butt, H.-J.; Fytas, G. Engineering the Hypersonic Phononic Band Gap of Hybrid Bragg Stacks. *Nano Lett.* **2012**, *12*, 3101−3108.
(33) Alonso-Redondo, E.; Huesmann, H.; El Boudouti, E.-H.; Tremel, W.; Djafari-Rouhani, B.; Butt, H.-J.; Fytas, G. Phoxonic Hybrid Superlattice. *ACS Appl. Mater. Interfaces* **2015**, *7*, 12488−12495.
(34) Cahill, D. G. Thermal Conductivity Measurement from 30 to 750 K: The 3ω Method. *Rev. Sci. Instrum.* **1990**, *61*, 802−808.
(35) Lee, S.-M.; Cahill, D. G. Heat Transport in Thin Dielectric Films. *J. Appl. Phys.* **1997**, *81*, 2590−2595.
(36) Xie, X.; Li, D.; Tsai, T.-H.; Liu, J.; Braun, P. V.; Cahill, D. G. Thermal Conductivity, Heat Capacity, and Elastic Constants of Water-Soluble Polymers and Polymer Blends. *Macromolecules* **2016**, *49*, 972−978.
(37) Xie, X.; Yang, K.; Li, D.; Tsai, T.-H.; Shin, J.; Braun, P. V.; Cahill, D. G. High and Low Thermal Conductivity of Amorphous Macromolecules. *Phys. Rev. B: Condens. Matter Mater. Phys.* **2017**, *95*, 35406.
(38) Habib, E.; Wang, R.; Wang, Y.; Zhu, M.; Zhu, X. X. Inorganic Fillers for Dental Resin Composites. *ACS Biomater. Sci. Eng.* **2016**, *2*, 1−11.
(39) Podgórski, M.; Becka, E.; Claudino, M.; Flores, A.; Shah, P. K.; Stansbury, J. W.; Bowman, C. N. Ester-Free Thiol−ene Dental restoratives—Part A: Resin Development. *Dent. Mater.* **2015**, *31*, 1255−1262.
(40) Kraft, P.; Eichenberger, W. Conception, Characterization and Correlation of New Marine Odorants. *Eur. J. Org. Chem.* **2003**, *2003*, 3735−3743.
(41) Dinh, C.-T.; Nguyen, T.-D.; Kleitz, F.; Do, T.-O. Shape-Controlled Synthesis of Highly Crystalline Titania Nanocrystals. *ACS Nano* **2009**, *3*, 3737−3743.
(42) Waite, J. H. Adhesion a La Moule. *Integr. Comp. Biol.* **2002**, *42*, 1172−1180.

DOI: 10.1021/acs.jpcc.7b08425
J. Phys. Chem. C 2017, 121, 25568−25575

(43) Lee, H.; Scherer, N. F.; Messersmith, P. B. Single-Molecule Mechanics of Mussel Adhesion. *Proc. Natl. Acad. Sci. U. S. A.* **2006**, *103*, 12999−13003.
(44) Danner, E. W.; Kan, Y.; Hammer, M. U.; Israelachvili, J. N.; Waite, J. H. Adhesion of Mussel Foot Protein Mefp-5 to Mica: An Underwater Superglue. *Biochemistry* **2012**, *51*, 6511−6518.
(45) Sparks, B. J.; Hoff, E. F. T.; Hayes, L. P.; Patton, D. L. Mussel-Inspired Thiol−Ene Polymer Networks: Influencing Network Properties and Adhesion with Catechol Functionality. *Chem. Mater.* **2012**, *24*, 3633−3642.
(46) Cheng, W.; Sainidou, R.; Burgardt, P.; Stefanou, N.; Kiyanova, A.; Efremov, M.; Fytas, G.; Nealey, P. F. Elastic Properties and Glass Transition of Supported Polymer Thin Films. *Macromolecules* **2007**, *40*, 7283−7290.
(47) Zhao, D.; Schneider, D.; Fytas, G.; Kumar, S. K. Controlling the Thermomechanical Behavior of Nanoparticle/Polymer Films. *ACS Nano* **2014**, *8*, 8163−8173.
(48) Ivanda, M.; Furić, K.; Musić, S.; Ristić, M.; Gotić, M.; Ristić, D.; Tonejc, A. M.; Djerdj, I.; Mattarelli, M.; Montagna, M.; et al. Low Wavenumber Raman Scattering of Nanoparticles and Nanocomposite Materials. *J. Raman Spectrosc.* **2007**, *38*, 647−659.
(49) Wood, A. B. *A Textbook of Sound: Being an Account of the Physics of Vibrations with Special Reference to Recent Theoretical and Technical Developments*; Macmillan: New York, 1930.
(50) Torrent, D.; Sánchez-Dehesa, J. Acoustic Metamaterials for New Two-Dimensional Sonic Devices. *New J. Phys.* **2007**, *9*, 323−323.
(51) Kim, D. J.; Kim, D. S.; Cho, S.; Kim, S. W.; Lee, S. H.; Kim, J. C. Measurement of Thermal Conductivity of TiO_2 Thin Films Using 3ω Method. *Int. J. Thermophys.* **2004**, *25*, 281−289.
(52) Lee, S.-M.; Cahill, D. G.; Allen, T. H. Thermal Conductivity of Sputtered Oxide Films. *Phys. Rev. B: Condens. Matter Mater. Phys.* **1995**, *52*, 253−257.
(53) Every, A. G.; Tzou, Y.; Hasselman, D. P. H.; Raj, R. The Effect of Particle Size on the Thermal Conductivity of ZnS/Diamond Composites. *Acta Metall. Mater.* **1992**, *40*, 123−129.
(54) Pietrak, K.; Winiewski, T. S. A Review of Models for Effective Thermal Conductivity of Composite Materials. *J. Power Technol.* **2015**, *95*, 14−24.
(55) Losego, M. D.; Moh, L.; Arpin, K. A.; Cahill, D. G.; Braun, P. V. Interfacial Thermal Conductance in Spun-Cast Polymer Films and Polymer Brushes. *Appl. Phys. Lett.* **2010**, *97*, 11908.
(56) Wen, J. Heat Capacities of Polymers. In *Physical Properties of Polymers Handbook*; Mark, J. E., Ed.; Springer: New York, 2007; pp 145−154.
(57) Saeedian, M.; Mahjour-Shafiei, M.; Shojaee, E.; Mohammadizadeh, M. R. Specific Heat Capacity of TiO_2 Nanoparticles. *J. Comput. Theor. Nanosci.* **2012**, *9*, 616−620.
(58) Prasher, R. Thermal Interface Materials: Historical Perspective, Status, and Future Directions. *Proc. IEEE* **2006**, *94*, 1571−1586.

DOI: 10.1021/acs.jpcc.7b08425
J. Phys. Chem. C 2017, 121, 25568−25575